Sombrero-shaped Fe3O4 nanoelements with tunable out-of-plane and in-plane magnetization components fabricated by nano-imprint lithography

Byung Seok Kwon, Zheng Li, Wei Zhang, and Kannan M. Krishnan

Citation: Journal of Applied Physics **115**, 17B506 (2014); doi: 10.1063/1.4862519
View online: http://dx.doi.org/10.1063/1.4862519
View Table of Contents: http://scitation.aip.org/content/aip/journal/jap/115/17?ver=pdfcov
Published by the AIP Publishing

JOURNAL OF APPLIED PHYSICS **115**, 17B506 (2014)

Sombrero-shaped Fe_3O_4 nanoelements with tunable out-of-plane and in-plane magnetization components fabricated by nano-imprint lithography

Byung Seok Kwon, Zheng Li, Wei Zhang,[a] and Kannan M. Krishnan[b]
Department of Materials Science and Engineering, University of Washington, Seattle, Washington 98195, USA

(Presented 8 November 2013; received 21 September 2013; accepted 22 October 2013; published online 23 January 2014)

We report on the magnetization structure of dish- and sombrero-shaped magnetite nanoelements fabricated via defect-free nanoimprint lithography and magnetron sputtering with controllable deposition flux. We demonstrate that as the sputtering time increases, the shape of the magnetite nanoelements evolves from a dish- to sombrero-shape due to the non-directionality of deposition. At remanence, the bottom layer of both nanoelements favors in-plane direction of magnetization driven by their shape anisotropy (aspect ratios $>$ 8:1). Micromagnetic modeling indicates that this bottom layer is a double vortex for the dish-shape but a single vortex pinned by the central cone in the sombrero-shaped nanoelement. In addition, unlike conventional nano-disks, however, both nanoelements have strong out-of-plane components at the edges; an additional out-of-plane component is also found at the center for the sombrero-shaped nanoelements. We conclude that these localized out-of-plane magnetization components are produced due to the complex shape of the elements. © *2014 AIP Publishing LLC*. [http://dx.doi.org/10.1063/1.4862519]

Fe_3O_4 (*magnetite*) nanoparticles owing to their bio-compatibility and room temperature ferrimagnetic behavior have been widely exploited in various biological and biomedical applications, including diagnoses such as magnetic resonance and/or magnetic particle imaging, and therapeutics such as targeted drug delivery for cancer, gene delivery, and/or hyperthermia.[1–6] Unlike most metallic ferromagnetic materials (e.g., Co, Ni), which oxidize and dissolve *in vivo*, Fe_3O_4 has demonstrated sufficient stability as well as an ability to be metabolized by the human body.[4] In order to test the performance of Fe_3O_4 *in vivo*, a reliable method for high quality, high-throughput, and low-cost production of Fe_3O_4 nanoparticles is necessary. Conventionally, Fe_3O_4 nanoparticles are synthesized using a "bottom-up" chemical route with very good and controllable size and size monodispersity.[1,7–9] However above ~25 nm in size, such methods pose difficulties in precisely controlling the shape, size and structure of the nanoparticles. To resolve these issues, a "top-down" fabrication method has been investigated and developed as an alternative approach.[10] Specifically, combining nanoimprint lithography (NIL)[11] and etching of a sacrificial layer, the fabrication and release of large-area, homogeneous lithographic nanoparticles have been demonstrated.[12] Recently, a defect-free patterning technique has also been demonstrated that utilizes flexible ethylene tetrafluoroethylene (ETFE) as a working stamp material, with advantages over rigid stamps made from silicon, glass, or quartz.[13] Such soft, polymer working stamps significantly increase the imprint-yield and pattern-quality, by inducing a conformal contact between the stamp and the substrate. The ETFE stamp can also be simply replicated via direct hot-embossing with a rigid master stamp. The replication and application of ETFE working stamps also increases the lifetime of the expensive master stamps. In addition, direct release of high-quality disk-shaped magnetic nanoparticles in solution was achieved by using a bilayer resist lift-off and substrate etching process.[13] These disk-shaped nanoparticles, consisting of Fe/Ta multilayers, lack good biocompatibility and favor an in-plane magnetization, due to their strong shape anisotropy. Such rigidness in their magnetization profile results in less flexibly in their detection and manipulation *in vivo*. As a result, magnetic nanoelements with sophisticated shapes and complex structures are being intensively investigated for improved magnetic response and functional behavior.[14,15] Here, we report the fabrication and magnetic properties of sombrero-shaped bio--compatible *magnetite* nanoelements, ~500 nm in diameter on a Si substrate, made by combined defect-free NIL and controlled non-directional deposition. During the process of fabrication, we found that as deposition time increases, the nanoelements evolve from dish- to sombrero-shaped nanoelements. These nanoscale elements with two different shapes were characterized using Magnetic Force Microscopy (MFM) for the remanent magnetization state and micromagnetic simulations. With distinct and tailored out-of-plane magnetization component at both the center and the edge, sombrero-shaped nanoelements, if subsequently released into solution, may give rise to advantageous magnetic response over conventional nano-disks in biomedical applications including, but not limited to, medical imaging applications.

We first fabricated ETFE replicas via hot-embossing a clean ETFE sheet (DuPont Tefzel) with a Si master mold (350 nm size holes in hexagonal lattice form, 250 nm groove depth, and 700 nm period, from Lightsmyth Technologies), using our previously developed recipes.[13] Next, we fabricated a bilayer resist undercut profile for metallization. The bilayer resist consists of an undercut layer, LOR 1A (MicroChem) and an imprint layer, NXR-1025 (Nanonex). After the thermal imprinting with the ETFE stamp, we performed oxygen-plasma reactive ion etching (RIE) to remove the imprint resist

[a]Present address: Argonne National Laboratory, Lemont, IL 60439, USA.
[b]Author to whom correspondence should be addressed. Electronic mail: kannanmk@uw.edu.

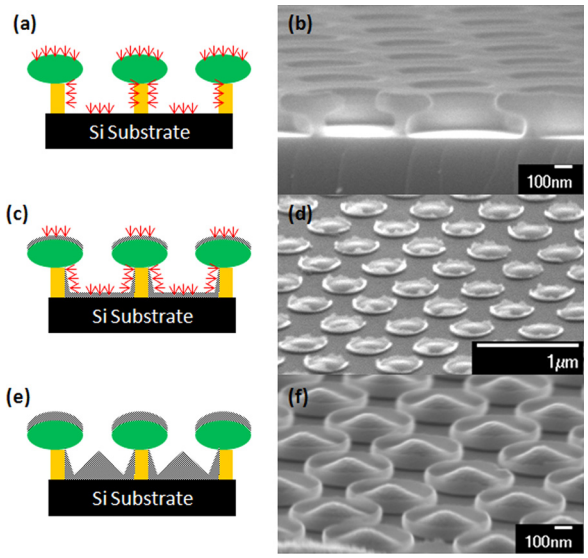

FIG. 1. Schematic diagram and SEM images of the development of NIL-patterned dish- and sombrero-shaped Fe_3O_4 nanoelements. (a) and (b) Bilayer undercut resist profile before deposition, (c) and (d) intermediate stage dish-shaped nanoelements, (e) and (f) final stage sombrero-shaped nanoelements.

residue, then selectively removed part of LOR 1A layer under the patterned area via wet-etching to create the bilayer-resist undercut profile (Figs. 1(a) and 1(b)). Next, we used non-directional deposition via magnetron sputtering to develop sombrero-shaped magnetite nanoelements (Figs. 1(c)–1(f)). At the initial stage, magnetron sputtering deposits materials at the bottom forming nearly uniform thickness, with only a small amount of materials deposited along the side-walls. As the deposition time increases, a peak at the center starts to develop, and the side-wall becomes more apparent, eventually forming the sombrero-shaped structures. We also note that these nanoelements, both dish- and sombrero-shaped, are ~500 nm rather than ~350 nm in size (feature size of the stamp). Such enlargement of the feature size is attributed to the undercut resist profile (Figs. 1(c)–1(f)). After deposition, lift off was performed to remove any organic resists and surplus metal on top, in order to achieve an array of ordered, isolated nanoelements on silicon substrate (Figs. 1(d) and 1(f)). We further conducted magnetic measurement in order to understand the magnetic properties of both dish- and sombrero-shaped nanoelements. MFM was used to analyze the preferred magnetization direction at remanent state and micromagnetic simulations were used to interpret the observed domain images at remanence.

Figure 1 shows the morphological evolution of the nanoelements at different stages of the deposition process. Figs. 1(a) and 1(b) demonstrate the bilayer undercut profile prior to deposition, by schematic illustration and SEM images, respectively. The nanolements evolve from dish- (Figs. 1(c) and 1(d)) to sombrero-shape (Figs. 1(e) and 1(f)). The bilayer resist undercut profile and non-directional deposition using magnetron sputtering are keys to create such shape of nanoelements. First, to fabricate dish- and sombrero-shape elements without defects, it is critical to control the time of RIE and wet etching to develop an undercut profile without any bottom tail or undercut resist residue due to under-etching.[16,17] To develop the nanoelements into two desired shapes, it is necessary to consider how non-directional deposition via magnetron sputtering is different from other deposition methods (e.g., evaporation, directional deposition via ion beam sputtering). For deposition techniques with high directionality and well-aligned target-substrate geometry, the side-wall deposition is usually minimized. However, for the magnetron sputtering used here, the deposition is quasi-isotropic with poor directionality and therefore the bilayer-resist undercut profile does not provide effective shielding to prevent the side-wall deposition. This leads initially to dish-shaped nanoelements after brief deposition (<90 min) and as sputtering time increases, we further observe accumulation of deposition at the center of each element into a cone shape. Further increase in deposition time (~480 min) leads to sombrero-shaped nanoelements with side-wall and a peak at the center (Figs. 1(e) and 1(f)).

MFM was used to analyze the out-of-plane magnetization state of both single dish- and sombrero-shaped nanoelements. An external field (~2500 Oe), perpendicular to the sample surface was applied for 20 s and then removed to achieve the magnetic remanent state. We first scanned for the topography using a CoCr coated low moment probe followed by a MFM scan with a lift height of 50 nm to investigate the magnetization state of both nanoelements. From the topography scan (Figs. 2(a) and 2(c)), we observe that both these nanoelements are ~500 nm in diameter and have side-walls with the sombrero-shaped nanoelement having a cone shaped structure at the center which is consistent with SEM images. From the MFM scan (Figs. 2(b) and 2(d)), we observe strong out-of-plane magnetic signal at the edge of both nanoelement and at the center peak of the sombrero-shaped nanoelement. For dish-shaped nanoelements, no out-of-plane magnetization in the center was observed.

To further investigate the magnetization state of both elements, micromagnetic simulation (LLG) was carried out[18] as schematically shown in Figs. 3(a) and 3(b). Following dimensions were used for simulations: the diameter of the nanoelement = 500 nm, the thickness of the disk-part = 50 nm, the

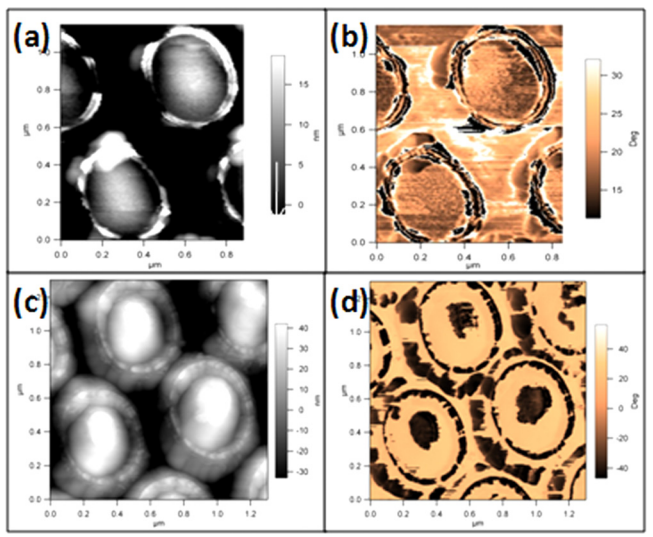

FIG. 2. AFM topography images for (a) dish- and (c) sombrero-shaped nanoelements. Corresponding MFM images for each element showing out of plane magnetization components at the side-wall for both nanoelements (b) and (d) and in the central cone for only the sombrero-shaped nanoelement (d).

thickness of the side-wall = 3 nm, the total height of side-wall = 150 nm, the diameter of top, and middle disk for sombrero-shaped nanoelement, 37.5 nm and 112.5 nm, the height of top, and middle disk for sombrero-shaped nanoelement, 50 nm. The following magnetic parameters were used for simulation: $M_s = 480$ emu/cm^3, exchange stiffness constant, $A = 1.32$ μerg/cm, magnetocrystalline anisotropy, $K_{mc} = 0$ to simulate the polycrystalline magnetite having $2 \times 2 \times 25$ nm^3 cell. An out-of-plane external field of 1500 Oe was applied and then removed to achieve the remanent state shown in (Figs. 3(c)–3(f)).The out-of-plane magnetization direction is shown by taking a side-view slice through the middle of each element. For the dish-shaped element, we observe a double vortex state for the bottom disk layer (Fig. 3(c)) with opposing chirality. This double vortex state influences the magnetic structure of the edge-wall due to strong exchange coupling, leading to an in-plane magnetization component at the edge-wall. In addition, a strong out-of-plane component was observed in the side-wall (side view (Fig. 3(g)) for a thickness of 3 nm (for larger thickness, ~5 nm, the magnetization in the side-wall was totally in plane). This is in agreement with the MFM images that where we observe an out-of-plane magnetization at the side-wall, thus we conclude the side-wall to be ~3 nm thick. Further, the MFM images revealed an in-plane magnetization at the center but the simulated double vortex state was not observed in MFM due to insufficient resolution. For sombrero-shaped nanoelements, however, the simulation predicts a single vortex state in the bottom disk component (Fig. 3(d)) with its magnetic singularity being pinned by the out-of-plane magnetization component of the central cone of the sombrero. Further, the magnetization state of vortex state of the disk is exchange-coupled to the side-walls (Fig. 3(f)). In addition, strong out-of-plane magnetization component at side-walls is predicted by the simulation (Fig. 3(h)) and observed in the MFM image. In conclusion, the remanent magnetization state of dish-shaped and sombrero-shaped nanoelements involves both in-plane and out-of-plane components that are consistent with their three-dimensional structures; and a good agreement was found between MFM images and micromagnetic simulation.

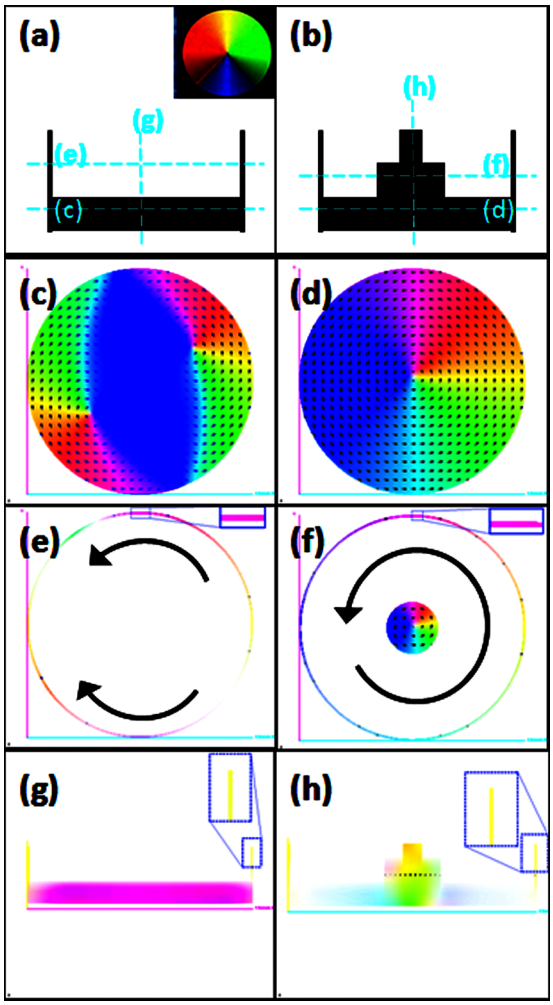

FIG. 3. Schematic diagram of the model of the (a) dish-shaped and (b) sombrero-shaped nanoelements used for LLG micromagnetic modeling. The dish-shape was modeled as a disk with a narrow ring on top. For the sombrero-shape, two additional disks with decreasing diameter were used to simulate the central cone as well. Domain structures were then simulated at different heights. The magnetic structure of the bottom disk component of (c) dish-shape shows a double-vortex structure with opposite chirality but (d) sombrero-shaped nanoelement shows a single vortex. The side-walls in both cases (e) and (f) show an in-plane component with the chirality consistent with the underlying disk due to strong exchange coupling. Cross-sectional view of (g) dish-shaped nanoelement with a strong in-plane component and (h) sombrero-shaped nanoelement with an out-of-plane component in the central cone. In both cases, the side-wall has an out-of-plane magnetization component.

In conclusion, we have demonstrated the fabrication and magnetic properties of the dish-shaped and sombrero-shaped Fe_3O_4 nanoelements with complex 3D magnetization structure. The dish- and sombrero-shaped nanoelements include different in-plane and out-of-plane magnetization components defined by their complex geometry. Specifically, the bottom layer of the sombrero-shaped element has a single vortex structure with its singularity pinned by the out-of- plane component of the central cone. In contrast, the dish-shaped nanoelement in remanence displays two vortices. Further work will include detailed hysteresis measurements and the release of the nanoparticles into solution after appropriate functionalization.

This work was supported by NSF-DMR under Grant No. 1063489. We thank Yufeng Hou and Dr. Andrew Lingley for helpful discussions. Nanoimprint work was performed at the MFF at University of Washington.

[1]R. M. Ferguson *et al.*, Med. Phys. **38**, 1619 (2011).
[2]K. M. Krishnan, IEEE Trans. Magn. **46**, 2523 (2010).
[3]H. Arami and K. M. Krishnan, IEEE Trans. Magn. **49**, 3500 (2013).
[4]M. Shinkai *et al.*, J. Magn. Magn. Mater. **194**, 176 (1999).
[5]M. M. Lin *et al.*, Nano Rev. **1**, 4883 (2010).
[6]C. Jimenez-Lopez *et al.*, J. Geophys. Res. **115**, G00G03, 10.1029%2F2009JG001152 (2010).
[7]I. Martínez-Mera *et al.*, Mater. Lett. **61**, 4447 (2007).
[8]R. Massart, IEEE Trans. Magn. **17**, 1247 (1981).
[9]K. V. Shafi *et al.*, Langmuir **17**, 5093 (2001).
[10]D. A. Canelas *et al.*, Wiley Interdiscip. Rev.: Nanomed. Nanobiotechnol. **1**, 391 (2009).
[11]S. Y. Chou *et al.*, J. Vac. Sci. Technol., B: Microelectron. Nanometer Struct.–Process., Meas., Phenom. **14**, 4129 (1996).
[12]W. Hu *et al.*, Nanotechnology **22**, 185302 (2011).
[13]W. Zhang and K. M. Krishnan, J. Appl. Phys. **111**, 07B509 (2012).
[14]J. S. Wi *et al.*, ACS Nano **5**, 6449 (2011).
[15]S. Tominaka and J.-S. Wi, J. Mater. Chem. **A1**, 330 (2013).
[16]W. Zhang *et al.*, J. Micromech. Microeng. **21**, 045024 (2011).
[17]W. Zhang *et al.*, J. Appl. Phys. **113**, 17B502 (2013).
[18]Z. Li and K. M. Krishnan, J. Appl. Phys. **113**, 17B901 (2013).